Hydraulic characteristics of the aeration basin in a ski-jump-step spillway

Shangtuo Qian and Jianhua Wu

ABSTRACT

The ski-jump-step spillway was designed using a ski-jump and an aeration basin to effectively pre-aerate flow in a stepped spillway. A new experimental study of the hydraulic characteristics of aeration basins was conducted to better understanding their pre-aeration properties and mechanisms. The plunge-pool patterns of aeration basins were classified into partially aerated, fully aerated, and vortex expelled, with increasing unit discharge. Relations between the distributions of the time-averaged pressure and the air concentration of the plunge-pools suggested that the ski-jump jet impact and the recirculating vortices are the main causes of plunge-pool air entrainment. Based on the export cross-section of the aeration basins, the bottom air concentrations remained greater than 3.0%. The sidewall air concentrations were greater than 7.5% and followed a logarithmic distribution in the vertical direction, demonstrating that the export flow attains a completely aerated state without any blackwater zones. In addition, increasing the aeration basin length was found to prevent the occurrence of a vortex expelled plunge-pool, thus promoting the appropriate pre-aeration effect under large unit discharges.

Key words | aeration basin, air entrainment, plunge-pool, pre-aeration, ski-jump-step spillway

Shangtuo Qian
College of Agricultural Engineering,
Hohai University,
Nanjing 210098,
China

Jianhua Wu (corresponding author)
College of Water Conservancy and Hydropower Engineering,
Hohai University,
Nanjing 210098,
China
E-mail: *jhwu@hhu.edu.cn*

NOTATION

a length of the steps (m)
B width of the chute (m)
b height of the steps (m)
C air concentration
D depth of the aeration basin (m)
g gravitational acceleration (m s^{-2})
z vertical coordinate from the spillway bottom (m)
h flow depth (m)
h_c critical flow depth (m)
L length of the aeration basin (m)
P time-averaged pressure (m)
Q flow discharge (m^3 s^{-1})
x horizontal distance from the start of aeration basin (m)

SUBSCRIPTS

b bottom
s sidewall

INTRODUCTION

In 21st century China, dozens of large-scale hydropower projects are continually being planned and constructed with rapidly developing construction techniques and materials, for example, roller compacted concrete (RCC) (Lian & Yang 2008; Cheng *et al.* 2012). The necessary release structures should be capable of handling floodwater releases under large unit discharges (Liu & Yang 2004; Xie *et al.*

doi: 10.2166/ws.2020.016

2016). Ski-jumps are a conventional option but require a large and costly energy dissipation basin downstream and might cause a serious atomization problem that is harmful to the environment and to human activities (Heller *et al.* 2005). Stepped spillways have become increasingly applied to cope with floodwater release because the RCC technique enables their economic and fast construction (Frizell & Mefford 1991; Chanson 1995; Chamani & Rajaratnam 1999). The main advantages of stepped spillways, in addition to construction economy and speed, are significant energy dissipation along the spillway to shorten the stilling basin downstream, intense flow aeration that reduces cavitation damage, and limited atomization (Boes & Hager 2003). However, a performance limitation of stepped spillways occurs predominantly under large unit discharges. Continuously increasing the unit discharge causes the point of the surface air inception to move downstream, before which there is a blackwater reach that is prone to cavitation damage (Hunt & Kadavy 2013; Meireles *et al.* 2014).

Many recent investigations involve extending the applicability of stepped spillways with respect to the upper unit discharge limitation. The bottom aerator, mounted at the first step of a stepped spillway, has been shown to be an effective technical means in this aspect; Pfister *et al.* (2006a, 2006b) were among the first to investigate the pre-aeration performance of the bottom aerator. The bottom aerator has been shown to successfully add an air layer near the step niches to help protect the spillway bottom against cavitation damage (Zamora *et al.* 2008). However, the bottom aerator can hardly stop the point of the surface air inception from moving downstream, highlighting the inevitable long blackwater reach during large unit discharges (Pfister *et al.* 2006a). The sidewalls within the blackwater reach continue to receive limited protection against cavitation damage because there is less air present in their vicinity (Zamora *et al.* 2008). Reviewing past hydropower engineering failures, the sidewalls of release structures probably suffer some cavitation damage, needing special attention and protection (Warnock 1947; Feng & Zhang 2008).

Inspired by the significant air entrainment caused by the interaction between a ski-jump jet and a plunge-pool, Qian *et al.* (2016) proposed the idea of using a ski-jump and an aeration basin to provide a well-pre-aerated flow for a stepped spillway downstream, and named the entire system a ski-jump-step spillway. The ski-jump and the aeration basin, which mainly play a role of pre-aeration and do not require considerations of energy dissipation efficiency, are designed with relatively small drop and size for acceptable time and cost of construction and for controlling the degree of atomization. The experiments by Qian *et al.* (2016) and Wu *et al.* (2016, 2020) offered preliminary, but overall direct, impressions regarding the hydraulic performance of the ski-jump-step spillway, exhibiting a total removal of blackwater reach and relatively high air concentrations in the stepped spillway section, even under large unit discharges (the maximum reached 118.00 m^2/s on the prototype). Accordingly, the ski-jump-step spillway is a promising solution to safely and effectively release floodwaters for large-scale hydropower projects.

The aeration basin, the key functional section of ski-jump-step spillways, generates a plunge-pool to receive the ski-jump jet and improve the flow aeration performance in the stepped spillway section downstream. Hydraulic characteristics of the aeration basin, notably the plunge-pool patterns, the distributions of time-averaged pressure and air concentration of the plunge-pools, and the air concentrations in the export cross-section that reflect the pre-aeration effect, are hotspot issues. The present study intends to experimentally explore these issues to better understand the properties and the mechanisms of pre-aeration using aeration basins.

EXPERIMENTAL SETUP AND METHODOLOGY

The laboratory experiments were conducted on a Plexiglas model of a ski-jump-step spillway at the High-Speed Flow Laboratory, Hohai University. Figure 1 is a definition sketch of the ski-jump-step spillway, which consisted of an entrance section, a ski-jump, a pre-step section, an aeration basin, and a stepped spillway section. The ski-jump-step spillway had a constant width B of 27.5 cm. The inlet had the profile of a standard waterways experimental station (WES) with a length of 33.0 cm and a height of 29.5 cm. The ski-jump was horizontal with a length of 33.0 cm. The pre-step and stepped spillway sections contained six and 16 steps respectively, and each step had a length a of

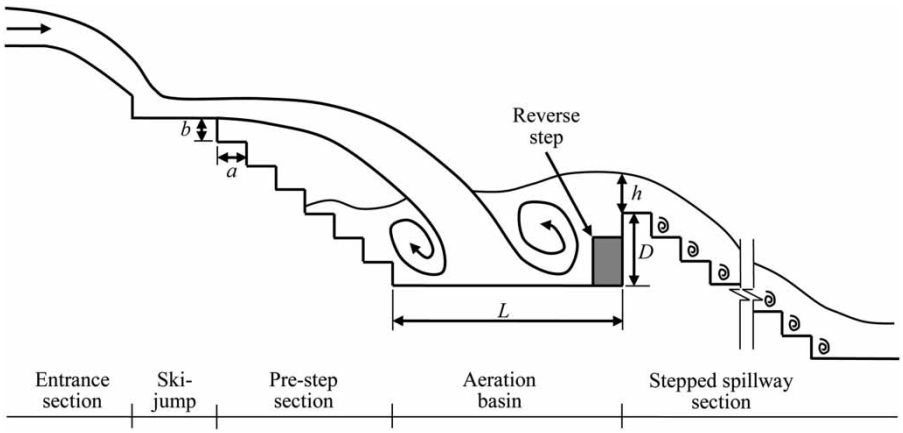

Figure 1 | Definition sketch of the ski-jump-step spillway.

11.0 cm and a height b of 9.0 cm. Two aeration basins with different lengths of $L = 88.0$ and 110.0 cm respectively were tested and named M1 and M2, respectively. Their depths remained consistent ($D = 27.0$ cm), and a reverse step was installed at the downstream end to stabilize the export flow.

The flow visualizations and hydraulic data measurements were carried out for a broad range of discharges $0.003 \leq Q \leq 0.128$ m^3/s, corresponding to the relative critical flow depths $0.24 \leq h_c/b \leq 3.12$, where h_c is the critical flow depth defined as $h_c = [(Q/B)^2/g]^{1/3}$, and g is gravitational acceleration. The flow depths (h) were measured with a manually operated pointer gauge placed in the export cross-section of the aeration basins. The time-averaged pressures (P) were measured using piezometers, the gauging points of which were placed along the bottom and sidewall (13.5 cm above the bottom) of the aeration basins with horizontal spacing of 10.0 cm. The air concentrations (C) were recorded by CQ6-2005 aeration apparatuses. Along the bottom and sidewall of the aeration basins, the gauging point locations of air concentration were the same as those of the time-averaged pressure. In the export cross-section of the aeration basins, one air concentration gauging point was placed on the bottom, and the other eight were placed on the sidewall with a vertical spacing of 5.0 cm.

The CQ6-2005 aeration apparatus, made by China Institute of Water Resources and Hydropower Research (IWHR), is a resistance-type instrument that collects and processes air concentration data by a microcomputer and paster-type sensors with a pair of parallel electrodes. The air concentration (C) was obtained by measuring the resistances in the aerated water (R_c) and in the clean water (R_o), according to the theory of Maxwell as follows: $C = (R_c - R_o)/(R_c + R_0/2)$.

RESULTS AND DISCUSSION

Plunge-pool patterns of aeration basins

The flow observations indicate that the plunge-pool patterns of the aeration basins are marked by a plunging ski-jump jet, large-scale recirculating vortices, and distinct air entrainment exhibiting a large amount of air bubbles mixed into the flow. According to the variations of the recirculating vortices and the air entrainment performance with unit discharge, the plunge-pool patterns are classified into partially aerated, fully aerated, and vortex expelled plunge-pools. Figure 2 shows the experimental photographs and definition sketches of these plunge-pool patterns, in which the photographs of the partially aerated, fully aerated, and vortex expelled plunge-pools were taken in M1 when $h_c/b = 0.61$, 1.31, and 2.59, respectively.

The partially aerated plunge-pool exists in the aeration basins during small unit discharges (Figure 2(a) and 2(b)). The ski-jump jet impacts and penetrates the plunge-pool, driving and separating counterclockwise and clockwise vortices, namely, the primary and secondary vortices, on its downstream and upstream sides, respectively. Air bubbles collect within a triangular region that contains the ski-jump jet and the recirculating vortices. Contrary to the ambient

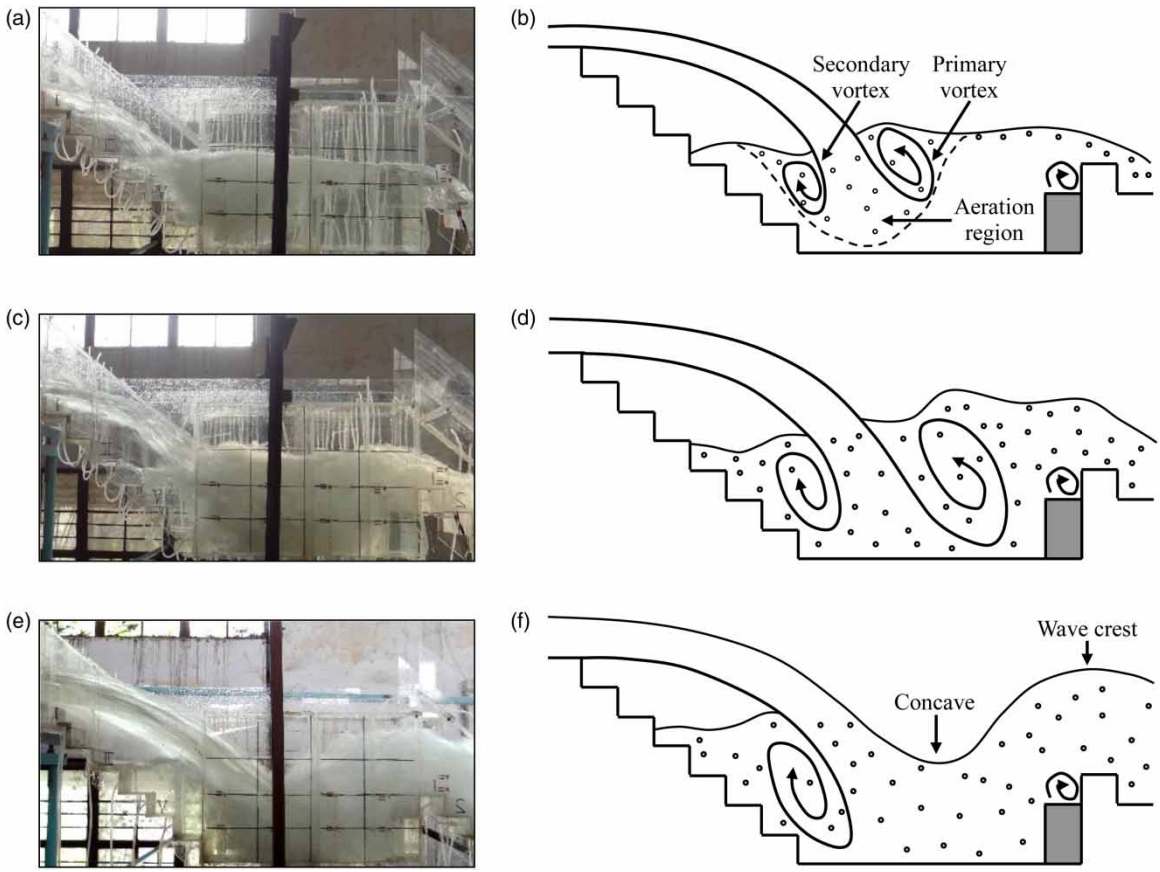

Figure 2 | Plunge-pool patterns: (a) and (b) partially aerated plunge-pool; (c) and (d) fully aerated plunge-pool; and (e) and (f) vortex expelled plunge-pool. The grey column represents the reverse step.

non-aeration fluid that seems essentially transparent, this triangular aeration region appears white from the air bubbles reflecting light (Wu 1989). The free surface of the plunge-pool stays stable both underneath and downstream from the ski-jump jet. Part of the air bubbles in the plunge-pool enter the stepped spillway section accompanying the export flow of the aeration basins.

With increasing unit discharge, the interaction between the ski-jump jet and the atmosphere increases, as do the sizes of the primary and secondary vortices. Accordingly, more air bubbles are entrained into the plunge-pool and the size of the aeration region gradually increases. As soon as the entire plunge-pool is dominated by the aeration region, showing a sufficient aeration state with a white color, the fully aerated plunge-pool begins to exist in the aeration basin (Figure 2(c) and 2(d)). The free surface of the plunge-pool remains stable underneath the ski-jump jet, while it shows a pseudoundular profile downstream from the ski-jump jet. Compared with that of the partially aerated plunge-pool, the export flow of the fully aerated plunge-pool carries many more air bubbles.

The vortex expelled plunge-pool exists in the aeration basins during large unit discharges (Figure 2(e) and 2(f)). The ski-jump jet has a large kinetic energy that cannot be sufficiently dissipated in the plunge-pool, thus expelling the primary vortex out of the aeration basins. Accordingly, the free surface of the plunge-pool forms a concave profile just downstream from the ski-jump jet impact; then, it is raised as a wave crest around the downstream end of the aeration basin. Compared with the partially and fully aerated plunge-pools, the vortex expelled plunge-pool highlights the violent turbulence characteristics signified by the fluctuating free surface and pulsating export flow that accompany flow ejections and sprays.

M1 exhibits a partially aerated plunge-pool for $h_c/b \leq 0.61$, a fully aerated plunge-pool for $0.93 \leq h_c/b \leq 2.05$, and

a vortex expelled plunge-pool for $h_c/b \geq 2.59$. By contrast, M2 exhibits partially and fully aerated plunge-pools for $h_c/b \leq 0.93$ and $h_c/b \geq 1.31$, respectively, never exhibiting a vortex-expelled plunge-pool within the experimental range of h_c/b. The differences between M1 and M2 demonstrate that increasing aeration basin length increases the critical onset unit discharges of the fully aerated and vortex expelled plunge-pools. With increasing aeration basin length, the size of the plunge-pool increases, thereby demanding larger recirculating vortices and more entrained air bubbles, which are associated with larger unit discharges to form the fully aerated plunge-pool. Meanwhile, increasing the aeration basin length dissipates the kinetic energy of the ski-jump jet and keeps the primary vortex away from the downstream end of the aeration basins, therefore preventing the occurrence of a vortex expelled plunge-pool.

Distributions of the time-averaged pressure and the air concentration in plunge-pools

Figure 3 shows the time-averaged pressures and the air concentrations measured along the bottom and sidewall for M1 and M2, where x is the horizontal distance from the start of the aeration basins.

With increasing h_c/b, the time-averaged pressures on the bottom and sidewall increase, and their distributions fluctuate more. The distributions are closely related to the enhanced ski-jump jet impact and plunge-pool turbulence, according to the observation of the plunge-pool patterns. The time-averaged pressure surges both in the first half and near the downstream end, which correspond to the impact of the ski-jump jet and the water level rise from the reverse step, respectively. In this study, the surge of the

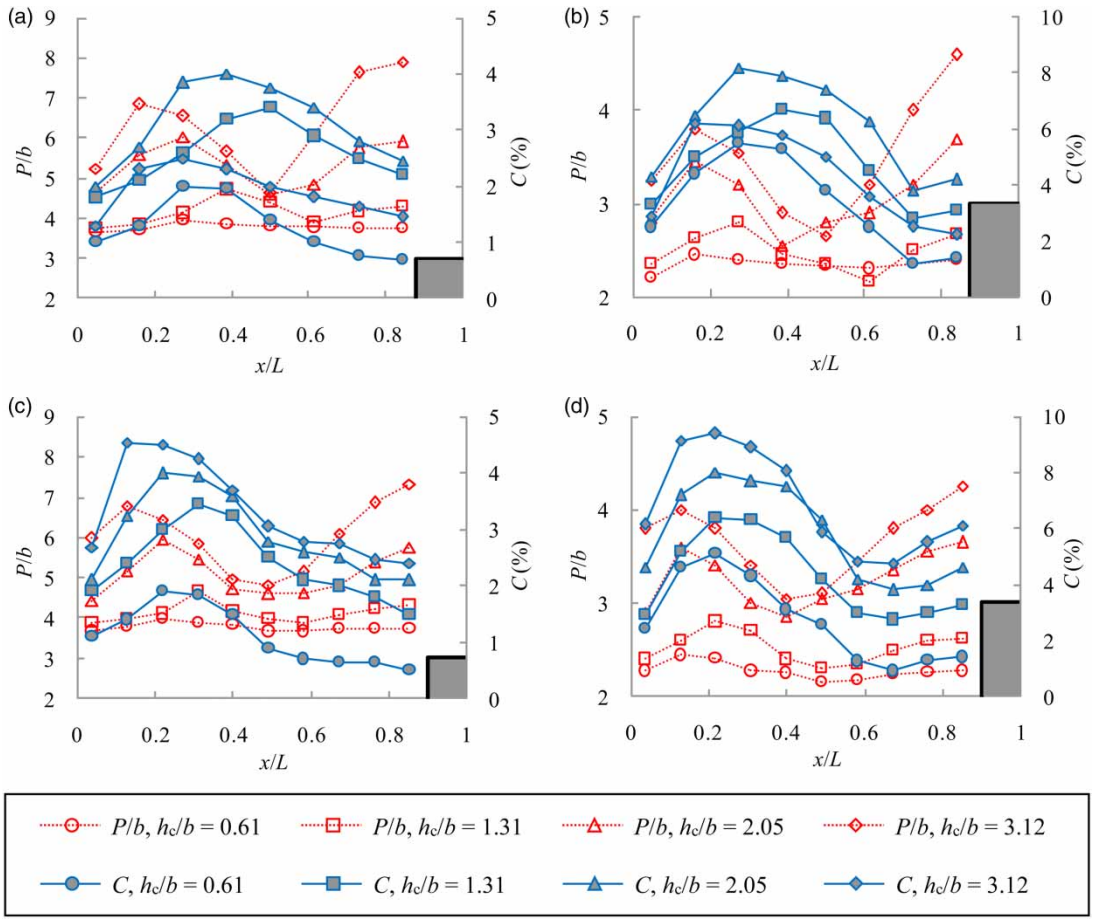

Figure 3 | Distributions of the time-averaged pressure and the air concentration in the plunge-pools: (a) along the bottom of M1; (b) along the sidewall of M1; (c) along the bottom of M2; and (d) along the sidewall of M2. The grey column represents the reverse step.

time-averaged pressure in the first half moves downstream and then upstream as h_c/b continuously increases, exhibiting the variation of the impact location of the ski-jump jet with unit discharge.

Notably, the bottom air concentration surges in the first half and craters near the downstream end. Contrariwise, the sidewall air concentration surges both in the first half and near the downstream end. Combining the distributions of the time-averaged pressure and the air concentration of the plunge-pools, the data show that the peak of air concentration in the first half coincides with the surging area of the time-averaged pressure caused by the impact of the ski-jump jet. Since numerous air bubbles collect around the ski-jump jet penetrating the plunge-pool, the ski-jump jet mixing with air and impacting the plunge-pool is speculated to be one of the important reasons for the plunge-pool air entrainment. There are also many air bubbles around and in the primary vortex developed downstream from the ski-jump jet. It is suggested that the primary vortex increases plunge-pool turbulence sufficiently to break the free surface and then bring about plunge-pool air entrainment. These entrained air bubbles are transported with the vortex recirculation, resulting in the sidewall air concentration surging near the downstream end. However, the relatively small bottom air concentration near the downstream end indicates that the primary vortex only barely drives the air bubbles to reach the bottom of the aeration basins.

With increasing h_c/b, the bottom and sidewall air concentrations of M1 first increase and then decrease, reaching their maximums just prior to the onset of the vortex expelled plunge-pool ($h_c/b = 2.05$), whereas those of M2 monotonously increase throughout the entire experimental range of h_c/b because of the absence of the vortex expelled plunge-pool. This indicated that the pulsating wave crest and random flow ejections and sprays that occur in the vortex expelled plunge-pool can result in significant air detachment from the plunge-pool in the aeration basins.

Air concentrations in the export cross-section of aeration basins

Figure 4 illustrates the bottom air concentrations C_b in the export cross-section of the aeration basins. In general, C_b is greater than 3.0% throughout the entire experimental range of h_c/b but shows differing h_c/b trends for M1 and M2. In the case of M1, C_b in the export cross-section decreases as h_c/b increases after reaching its maximum when $h_c/b = 2.05$. In the case of M2, C_b in the export cross-section reaches its maximum when the greatest $h_c/b = 3.12$ and can be described as follows:

$$C_b = 0.039(h_c/b)^{0.775} \quad (1)$$

For a stepped spillway with a bottom aerator, Pfister *et al.* (2006b) determined $C_b(h_c/b)$ immediately downstream of the air cavity, which is also plotted in Figure 4, as follows:

$$C_b = 0.1(h_c/b)^{-1} \quad (2)$$

Accordingly, the pre-aeration effect of the bottom aerator continuously decreases as h_c/b increases, thus becoming limited under large unit discharges.

Figure 5(a) shows the sidewall air concentration distributions $C_s(z/h)$ in the export cross-section of the aeration basins, where z is the vertical coordinate from the spillway bottom. These values of C_s generally increase as z/h increases; the smallest value is 7.5%. In the export cross-section, C_s and C_b exhibit the same trends with h_c/b; as a result, they appear larger for M2 than for M1 since $h_c/b >$ 2.5, indicating that the increase in the aeration basin length is favorable for improving the pre-aeration effect of the aeration basins under large unit discharges, as explained below. When the vortex expelled plunge-pool exists in the aeration basins, the air detachment of the plunge-pool, which results from the pulsating wave crest and random

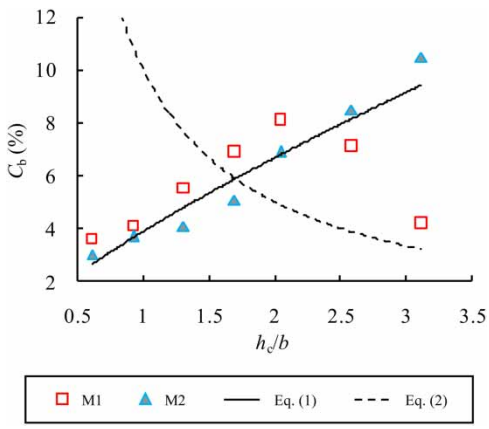

Figure 4 | Bottom air concentrations in the export cross-section of aeration basins.

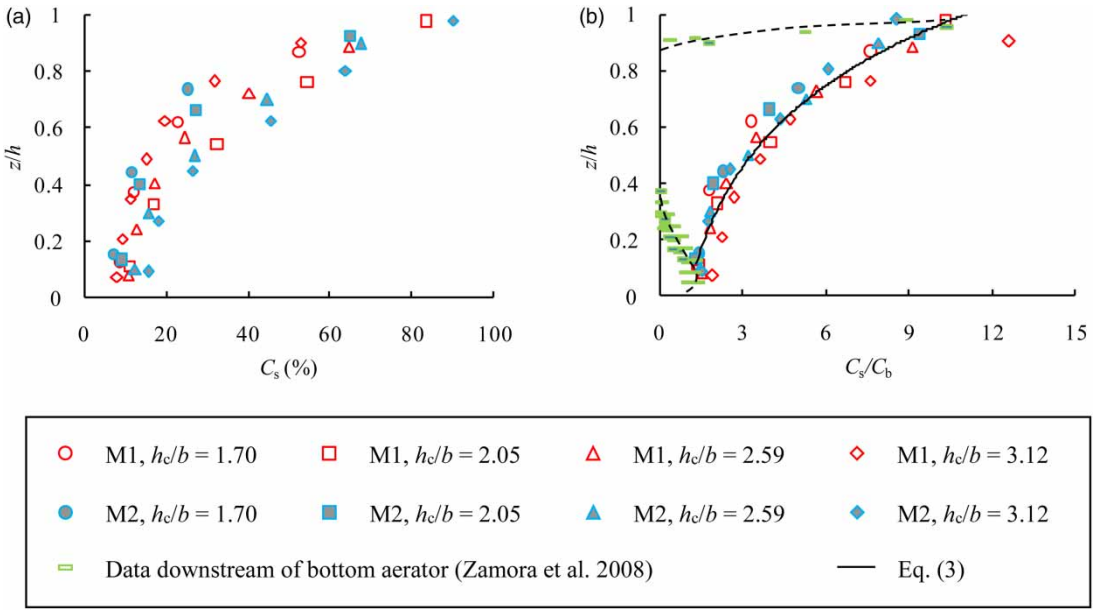

Figure 5 | Sidewall air concentrations in the export cross-section of the aeration basins: (a) $C_s(z/h)$; (b) $C_s/C_b(z/h)$.

flow ejections and sprays, is enhanced as the unit discharge increases. By avoiding the occurrence of the vortex expelled plunge-pool, the increase in the aeration basin length causes the air entrainment performance of the aeration basins to continuously increase as the unit discharge increases, bringing about the appropriate pre-aeration effect for the stepped spillway section under large unit discharges.

The sidewall air concentration distributions in the export cross-section of the aeration basins are further presented in Figure 5(b). Using the coordinates C_s/C_b and z/h, a unified curve for M1 and M2 under various h_c/b conditions is plotted. The resulting curve follows a logarithmic function with $R^2 = 0.936$ as follows:

$$C_s/C_b = 0.415 \ln (z/h) + 0.001 \quad (3)$$

Consequently, the entire sidewall beneath the free surface of the export flow is well-aerated to protect against cavitation damage. Zamora *et al.* (2008) experimentally measured the air concentration distributions with the step immediately downstream of the bottom aerator in the stepped spillways; the data are collected and shown in Figure 5(b) for comparison. The typical air concentration profile from the presence of the bottom aerator suggests that the flow cross-section is divided into three parts: the self-entrained air layer from the free surface, the thin diffusion air layer by the bottom aerator, and the blackwater zone sandwiched between them. Note that the blackwater zone can cause cavitation damage on the nearby sidewalls.

CONCLUSIONS

Specifically designed experiments were conducted to better understand the plunge-pool patterns and the pre-aeration properties and mechanisms of the aeration basin in a ski-jump-step spillway.

The plunge-pool patterns of the aeration basins are classified into partially aerated, fully aerated, and vortex expelled, as the unit discharge increases. The vortex expelled plunge-pool is especially significant because of the fluctuating free surface and pulsating export flow that accompany flow ejections and sprays, which are detrimental to pre-aeration under large unit discharges and may result in atomization problems. The discharge thresholds between different plunge-pool patterns rise proportionately as the aeration basin length increases, providing a way to prevent the occurrence of the vortex expelled plunge-pool.

By establishing the relationships between the distributions of the time-averaged pressure and the air concentration of the plunge-pools, the data suggests that the ski-jump jet mixing with air and impacting the plunge-pool and the large-scale

recirculating vortices are the main reason for the plunge-pool air entrainment. If the vortex expelled plunge-pool is prevented in the aeration basins, the bottom and sidewall air concentrations in the export cross-section could continuously increase with unit discharge, bringing about the appropriate pre-aeration effect of the aeration basins under large unit discharges. These sidewall air concentrations follow the unified logarithmic distribution expressed by Equation (3) in the vertical direction, indicating that the export flow of the aeration basins attains a completely aerated state without any black-water zones close to the spillway bottom and sidewalls. To the best of our knowledge, the former advantages in pre-aeration are not achieved by other pre-aeration facilities such as the bottom aerator.

As the aeration basin length decides the engineering feasibility and influences the flow pattern and pre-aeration performance, further studies are encouraged to establish their detailed function relations and provide guidance for preliminary designs.

ACKNOWLEDGEMENTS

The authors acknowledge the financial support of the National Natural Science Foundation of China (Grant No. 51479057 and 51809079), the Fundamental Research Funds for the Central Universities (Grant No. 2019B18414), and the China Postdoctoral Science Foundation (Grant No. 2018M632218).

REFERENCES

Boes, R. M. & Hager, W. H. 2003 Hydraulic design of stepped spillways. *Journal of Hydraulic Engineering* **129** (9), 671–679. doi:10.1061/(ASCE)0733-9429(2003)129:9(671).

Chamani, M. R. & Rajaratnam, N. 1999 Characteristics of skimming flow over stepped spillways. *Journal of Hydraulic Engineering* **125** (4), 361–368. doi:10.1061/(ASCE)0733-9429(1999)125:4(361).

Chanson, H. 1995 *Hydraulic Design of Stepped Cascades, Channels, Weirs and Spillways*. Oxford, Pergamon, UK.

Cheng, C. T., Shen, J. J., Wu, X. Y. & Chau, K. W. 2012 Operation challenges for fast-growing China's hydropower systems and respondence to energy saving and emission reduction. *Renewable & Sustainable Energy Reviews* **16** (5), 2386–2393. doi:10.1016/j.rser.2012.01.056.

Feng, Y. X. & Zhang, X. S. 2008 Research and implementation on aeration in cavitation-protection for the sidewalls of Ertan spillway tunnel. In: *International Conference on Dam Safety Management*, Nanjing, China.

Frizell, K. H. & Mefford, B. W. 1991 Designing spillways to prevent cavitation damage. *Concrete International* **13** (5), 58–64.

Heller, V., Hager, W. H. & Minor, H.-E. 2005 Ski jump hydraulics. *Journal of Hydraulic Engineering* **131** (5), 347–355. doi:10.1061/(ASCE)0733-9429(2005)131:5(347).

Hunt, S. L. & Kadavy, K. C. 2013 Inception point for embankment dam stepped spillways. *Journal of Hydraulic Engineering* **139** (1), 60–64. doi:10.1061/(ASCE)HY.1943-7900.0000644.

Lian, J. J. & Yang, M. 2008 *Hydrodynamics for High Dam*. China Water Power Press, Beijing, China (in Chinese).

Liu, C. & Yang, Y. Q. 2004 Study on air entrainment to alleviate cavitations at the end of anti-arc in spillway tunnel. *Journal of Hydrodynamics* **19** (3), 375–382. doi:1000-4874(2004)03-0375-08 (in Chinese).

Meireles, I. C., Bombardelli, F. A. & Matos, J. 2014 Air entrainment onset in skimming flows on steep stepped spillways: an analysis. *Journal of Hydraulic Research* **52** (3), 375–385. doi:10.1080/00221686.2013.878401.

Pfister, M., Hager, W. H. & Minor, H.-E. 2006a Stepped chutes: pre-aeration and spray reduction. *International Journal of Multiphase Flow* **32** (2), 269–284. doi:10.1016/j.ijmultiphaseflow.2005.10.004.

Pfister, M., Hager, W. H. & Minor, H.-E. 2006b Bottom aeration of stepped spillways. *Journal of Hydraulic Engineering* **132** (8), 850–853. doi:10.1061/(ASCE)0733-9429(2006)132:8(850).

Qian, S. T., Wu, J. H. & Ma, F. 2016 Hydraulic performance of ski-jump-step energy dissipater. *Journal of Hydraulic Engineering* **142** (10), 05016004. doi:10.1061/(ASCE)HY.1943-7900.0001178.

Warnock, J. E. 1947 Cavitation in Hydraulic Structures: A Symposium: Experiences of the Bureau of Reclamation. *Transactions of the American Society of Civil Engineers* **112** (1), 43–58.

Wu, C. G. 1989 *Air–Water Flow in Open Channel*. Chengdu University of Science and Technology Press, Chengdu, China (in Chinese).

Wu, J. H., Qian, S. T. & Ma, F. 2016 A new design of ski-jump-step spillway. *Journal of Hydrodynamics* **28** (5), 914–917. doi:10.1016/S1001-6058(16)60692-3.

Wu, J. H., Qian, S. T., Wang, Y. & Zhou, Y. 2020 Residual energy on ski-jump-step and stepped spillways with various step configurations. *Journal of Hydraulic Engineering* **146** (4), 06020002.

Xie, S. Z., Wu, Y. H. & Chen, W. X. 2016 New technology and innovation on flood discharge and energy dissipation of high dams in China. *Journal of Hydraulic Engineering* **47** (3), 324–336. doi:10.13243/j.cnki.slxb.20150984 (in Chinese).

Zamora, A. S., Pfister, M., Hager, W. H. & Minor, H.-E. 2008 Hydraulic performance of step aerator. *Journal of Hydraulic Engineering* **134** (2), 127–134. doi:10.1061/(ASCE)0733-9429(2008)134:2(127).

First received 24 September 2019; accepted in revised form 19 January 2020. Available online 7 February 2020